International Journal of Steel Structures
https://doi.org/10.1007/s13296-022-00679-y

Online ISSN 2093-6311
Print ISSN 1598-2351

Cyclic Inelastic Behavior of Plate Welded to Concrete-Filled Circular Hollow Section

Xiaone Wei[1] · Michel Bruneau[2]

Received: 26 February 2022 / Accepted: 23 September 2022

Abstract
An experimental study was conducted to investigate the tensile strength of a gusset plate connected to the steel surface of a Concrete Filled Tube (CFT) segment, as this could be a simple detail appealing when connecting braces to CFT bridge columns in a seismic retrofit perspective (or even for new design). Sixteen specimens were built with various concrete-filled Circular Hollow Section sizes, as well as different thicknesses of the longitudinal gusset plate (a.k.a. branch plate). Monotonic and cyclic tests were performed on these specimens, for which the failure modes and ultimate strength of the connections are presented. The failure strengths from the experiments are compared with the analysis results obtained from finite element models. Results from this comparison are found to generally match with each other. However, hysteretic behavior is found to be deficient and it is recommended to keep this connection elastic if used for seismic design purpose.

Keywords Concrete-filled circular hollow section · Gusset/branch plate · Inelastic cyclic test · Tensile strength · Failure

1 Introduction

The benefits of the composite behavior provided by composite Concrete Filled Steel Tube (CFT) columns in buildings have been well established decades ago (e.g., Bauer, 1988; Tarics, 1972; Viest et al., 1997; Webb & Peyton, 1990), and even in nonbuilding applications (Vogeli, 1950). Implementations in bridges remain few (e.g., Han et al., 2014; Huang, 2015; Kerensky & Dallard, 1968; Mori et al., 2015), but are foreseen to increase on the strength of research that has demonstrated the ductile behavior of such composite CFT columns as a means towards satisfactory seismic performance (Hajjar, 2000; Hajjar et al., 2013; Lai et al., 2017; Leon et al., 2007; Marson & Bruneau, 2004; Montejo et al., 2012; Roeder et al., 2009, 2010;). Recent research has also shown the advantages of considering the full flexural and shear composite strength of CFT in drilled shaft applications (Kenarangi & Bruneau, 2019a, 2019b, 2020; Moon et al., 2013; Xiao et al., 2012), often used in bridges. Research highlighting the multi-hazard benefits of composite CFT columns (e.g., Imani et al., 2015, Fouche et al., 2017; Saini & Shafei, 2019) is also anticipated to accelerate acceptance of composite CFT columns by bridge engineers.

However, the conventional approach investigated so far has consisted of relying of the hysteretic energy dissipation of bridge columns to provide seismic resistance. Alternatively, Wei and Bruneau (2016a) investigated the feasibility of using Buckling Restrained Braces (BRBs) as structural fuses between the columns of bridge bents. This improved the bents' seismic resistance and minimized the induced damage and repairs to the bridge. This therefore results in more resilient bridges because they can remain in service following earthquakes. For this purpose, it was observed that using composite CFT columns in these bridge braced bents could be advantageous. These CFT columns have more strength and lower stiffness compared to Reinforced Concrete (RC) columns (as they could be of smaller diameter for the required strength), which makes it easier to achieve a structural-fuse objective (Vargas & Bruneau, 2006).

For this purpose, a gusset plate running through the entire column and welded to both sides of the CFT would provide a robust and effective detail to connect the BRBs to the CFT columns. However, that is an intrusive detail and questions arose as to what strength and inelastic response could be developed if instead the gusset plates were only welded to

✉ Xiaone Wei
xiaonewe@buffalo.edu

[1] Michael Baker International, Chicago, IL 60606, USA

[2] Department of Civil, Structural, and Environmental Engineering, University at Buffalo, Amherst, NY 14260, USA

Published online: 11 October 2022

the steel Circular Hollow Section (CHS) of the CFT on the face where the BRBs were connected. Incidentally, such a significantly simpler detail could also be useful if adding BRBs to a retrofitted bridge having steel-jacketed RC columns. In both cases, an axial tension force, N, is applied by the gusset plate (a.k.a. "branch plate") perpendicular to its surface to the CFT. As shown in Fig. 1a, the presence of the concrete inside the CHS prevents the side faces of the steel shell from deforming into a more significant oval shape. Therefore, the perpendicular pulling force N that can be resisted by the CFT column may be larger than when connecting to a hollow CHS itself (Fig. 1b) of the same thickness and diameter. Also, given that the axial force could come from a BRB that is subjected to cyclic demands during an earthquake, a question arose as to whether this connection detail could provide some level of stable hysteretic behavior or if such cyclic inelastic action should be strictly avoided.

2 Prior Connection Research

Note that this connection detail could also benefit other applications, for which further knowledge on its strength and behavior could be valuable. Also, note that when the load from the BRB reverses, this connection is subjected to compressive force, but the concrete infill will directly resist this compressive force. In other words, the connection under tension loading controls the connection design, and this is the issue investigated here. Note that although the focus in this paper is on tensile loading transmitted through this kind of connection to composite CFT column, the connection in actual applications may also experience shear loading (i.e., perpendicular to the tensile loading direction); this would be included in a subsequent stage of study if satisfactory tension behavior (explored here) is first obtained.

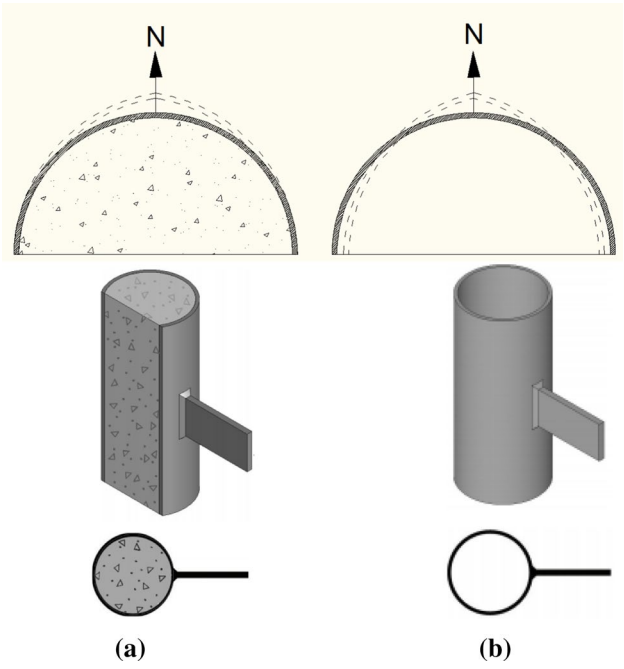

Fig. 1 Deformation under perpendicular tension loading N from branch plate: **a** CFT; **b** CHS (adapted from Voth, 2010)

There has been considerable analytical and experimental research conducted to investigate the strength and failure behavior of a branch plate welded to a hollow CHS (Fig. 1b). Wardenier et al. (2010) pointed out that the ultimate branch plate-to-CHS connection resistance in that case is related to two governing CHS limit states, namely: CHS plastification (with large axial and flexural plastic deformations) and CHS punching shear. While concrete (or grout) filling in the Rectangular Hollow Section (RHS) has been investigated as a stiffening method to improve the connection strength to branch plates (Packer, 1995), limited research has been conducted to investigate the concrete filled branch plate-to-CHS connection strength and failure mode (and none has investigated cyclic inelastic response). For grouted filled CHS under branch member tension loading, Wardenier et al. (2008) suggested using Eq. 1 from API (2007) to calculate the connection punching shear resistance. Voth (2010) adapted Eq. 1 into Eq. 2 for grouted filled branch plate-to- CHS connections, when the branch plate is loaded by a perpendicular tension force:

$$N_1^* = 0.36\pi d_1 f_{y0} t_0 \frac{k_a}{sin\theta_1} \tag{1}$$

$$N_1^* = 0.72 f_{y0} l_1 t_0 \tag{2}$$

where: f_{y0} is the yield strength of the steel material of the CHS, l_1 is the welded length of the branch plate along the wall of CHS, t_0 is the thickness of the CHS, d_1 is the diameter of the branch member CHS, θ_1 is the angle between the branch CHS member to the main CHS member and k_a equals to $\left(1 + sin\theta_1\right)/\left(2sin\theta_1\right)$.

Voth (2010) performed a parametric study of various branch plate-to-CHS connection behaviors using finite element models, and also tested twelve hollow specimens to verify their failure strengths and modes. Four additional specimens were filled with grout, including two having the branch plate configuration shown in Fig. 1a. For the CHS in these grout-filled specimens, the diameter and wall thickness were 8.625″ and 0.189″, respectively. Test results showed that the grout filling significantly increased the tensile strength of the connection when compared with same-size CHS specimens with no filling. Punching shear failure governed the capacity, when the CHS deformation at the branch plate's connection was beyond 3% of the CHS diameter. Only two specimens were tested, so experimental results

were limited. Design equations for grout-filled CHS with branch plate connections were not proposed. To fill the gaps in knowledge on the behavior and failure strength of this kind of connection to CFT columns, experimental research was conducted. Quasi-static monotonic and cyclic tests were performed on 16 specimens having branch plates welded to CFTs with various CHS diameters (and diameters mostly larger than previously tested), to investigate this behavior and connection strength. Test results were compared with finite element models of the specimens built in *Abaqus Version 6.14*. A summary of this work (Wei & Bruneau, 2016b) is presented here.

3 *Abaqus* Specimen Model and Results

Abaqus models were constructed to predict behavior of the specimens. These models considered that the force from the branch plate was applied to the concrete-filled CHS through the fillet welds of the branch plate to the CHS. Preliminary analyses with trial models showed that this effect, and even the width of the fillet welds, had a significant impact on the predicted strength of the specimens.

The *Abaqus* model of the specimen includes the concrete-filled CHS, the branch plate, and the fillet weld (Fig. 2a). Taking advantage of symmetry to reduce the computational

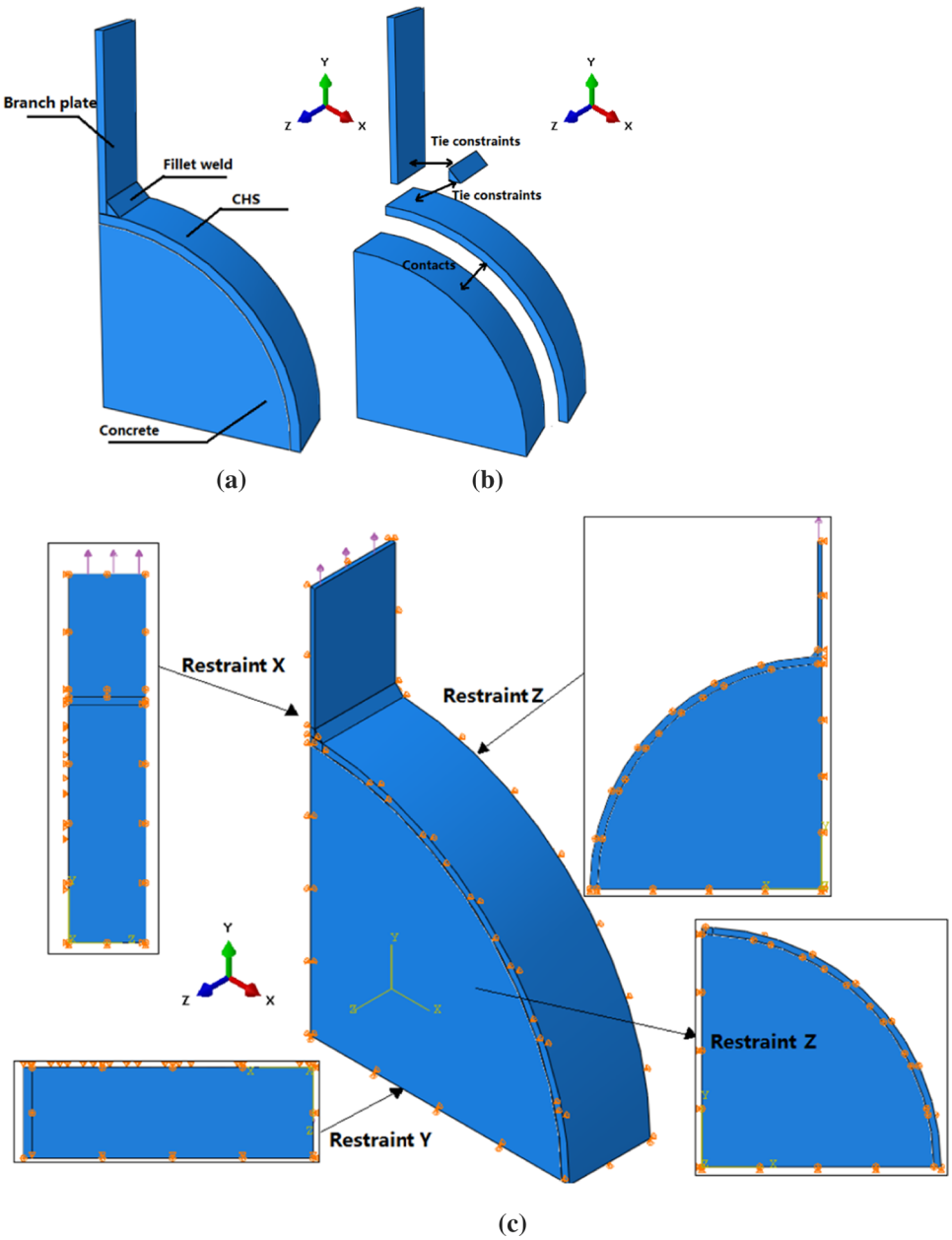

Fig. 2 *Abaqus* model for an example specimen: **a** parts; **b** constraints and contacts between parts; **c** restraints

demand, only 1/8 of the specimen was modeled. The bolted tab-to-branch plates connection was not modeled, and uniform area loads were applied at the tip of the branch plate. Each component of the *Abaqus* model in Fig. 2 was modeled using the general-purpose solid element C3D8R. Tie constraints were used to model the fillet weld in contact with both the CHS and the branch plate (Fig. 2b). "Surface to surface" constraints were used to discretize the ties. The load was transferred from the branch plate to the CHS through the fillet weld. A friction formulation set to be "penalty" was used to model the general contact between the outer surface of the concrete infill and the inner surface of the CHS; directionality was set as "isotropic". Per Rabbat and Russell (1985), the friction coefficient between the steel and the infilled concrete was set equal to 0.57.

A concrete infill compressive strength of 4.05 ksi was used, corresponding to the average value obtained from concrete cylinders tests of the concrete cast in the specimens. The concrete was defined to have an elastic modulus of 3605 ksi and a Poisson ratio of 0.2. The concrete tensile strength of 0.41 ksi was obtained from $f_t = 6.5\sqrt{f'_c}$. A concrete damage plasticity (CDP) material model was used; its two main failure mechanisms were defined as tensile cracking and compression crushing. The shape of the yield surface for the CDP model used in *Abaqus* was defined with parameters set to the following values: (a) Ratio of distances between the hydrostatic axis and the compression and tension meridian in the deviatoric cross section, $K_c = 0.67$; (b) Plastic potential eccentricity factor (length of the segment between the vertex of the hyperbola and its center) = 0.01; (c) Ratio between the strength of concrete in its biaxial state of stress, f_{bo}, and its uniaxial state of stress, f_{co}, = 1.16; (d) Dilation angle = 38°; (e) Viscosity parameter = 0.002. CHS steel material properties were defined by data from coupon tests (with values obtained for each type and size of CHS used). These properties are presented later in Table 2. A572Gr60 steel, with yield strength of 60 ksi and ultimate strength of 75 ksi, was used for the branch plates. An E80 matching electrode, with yield and ultimate strength of 68 and 80 ksi, respectively, was used for all fillet welds.

Nominal engineering stress and strain obtained were converted into true stress and strain. Boundary conditions for different elements of the specimen model are shown in Fig. 2c where, for each of the blown-up surface, the directions in which those surfaces have been restrained are indicated. Note that since only 1/4 of the branch plate was modeled in *Abaqus* (as shown in Fig. 2), the forces on the branch plate obtained from the *Abaqus* model have been multiplied by 4 to be compared with those experimentally obtained.

Displacement control was used to gradually apply displacements at the branch plate, until failure occurred in the model, defined as when the ultimate strain indicated by the true stress and strain material model was reached in the CHS. Note that the true stress and strain material model was derived based on the coupon tests of CHS used in each specimen. Large-displacement theory was considered. The specifics for the meshing are not described here due to space constraints (these details are presented in Wei & Bruneau, 2016b).

The specimen's controlling section is defined as where the highest stress/strain was first reached in the extreme fiber. This section was found located in the CHS close to the weld, as shown by the arrows in the enlarged view in Fig. 3b. The first-yield strength of the specimen was defined as the point when the extreme fiber of this controlling CHS section reached the yield true stress (marked by the dot in line with the branch plate in the enlarged view in Fig. 3b). The corresponding Von-Mises stress contours for the specimen are shown in Fig. 3a). Results from these finite element analyses are presented together with the experimental results in subsequent sections.

4 Concrete-Filled CHS Specimen and Test Setup

The test setup shown in Fig. 4 was used to test the concrete-filled CHS specimens. A reaction frame available in the Structural Engineering and Earthquake Simulation Laboratory (SEESL) was used to support the actuator that was used to load the specimen. This actuator was connected to one side of the specimen; the other side of the specimen was connected to a reaction block, itself bolted down to a floor beam of the reaction frame using threaded bars. At the actuator and at the reaction block, one line of ¾" slip-resistant A490 bolts was used to connect the plates extending from the specimen (branch plates) to double sets of plate (tab plates), as shown in Fig. 5. In the reaction frame, a wood block was used between the floor beam and the specimen to support the specimen's self-weight. A PTFE/Teflon plastic sheet was inserted between the specimen and the wood block to reduce the risk of friction forces developing between them. Guiding blocks were used on each side to secure the specimen and avoid instability of the test setup in the out-of-plane loading direction. Beam clamps were used to fix the two guiding blocks to the floor beam.

Figure 5 shows the fillet welds between the CHS and the branch plate, as well as the bolt connections between the branch and tab plates. Double-sided fillets were used to weld the branch plates to the CHS before concrete was poured into the CHS. Concrete for all specimens was cast at the same time, from the same mix. A regular concrete was used. The specimens were cast horizontally and no surface finish was applied. Shrinkage of the concrete was not an issue as the specimens were tested after concrete had cured 28 days. The

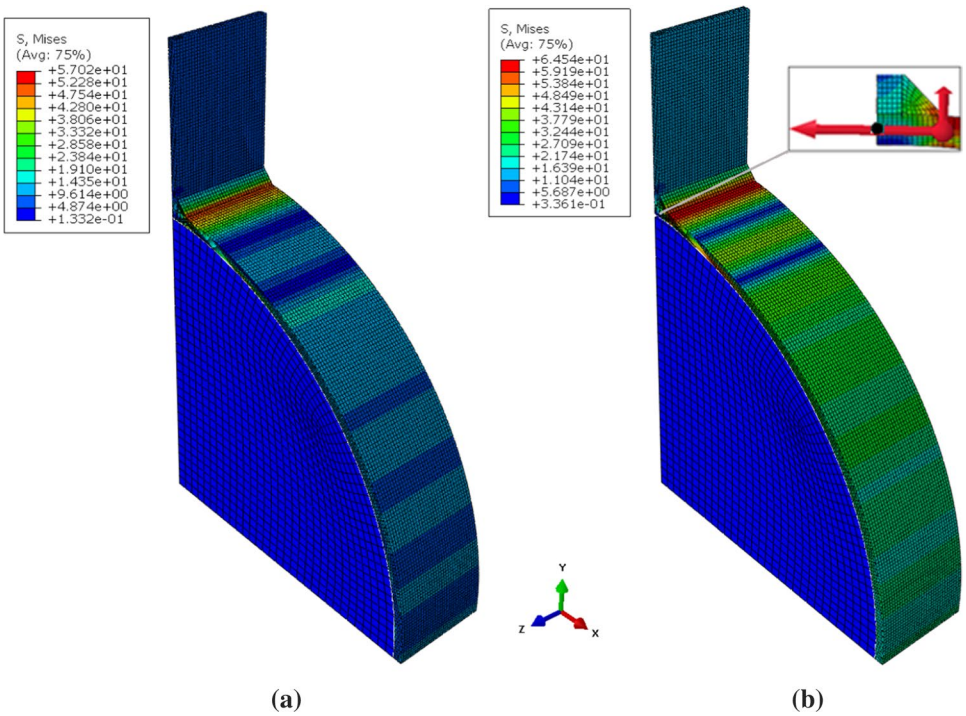

Fig. 3 Von-Mises stresses from *Abaqus* model of specimen (unit: ksi): **a** at first yielding; **b** at maximum moment

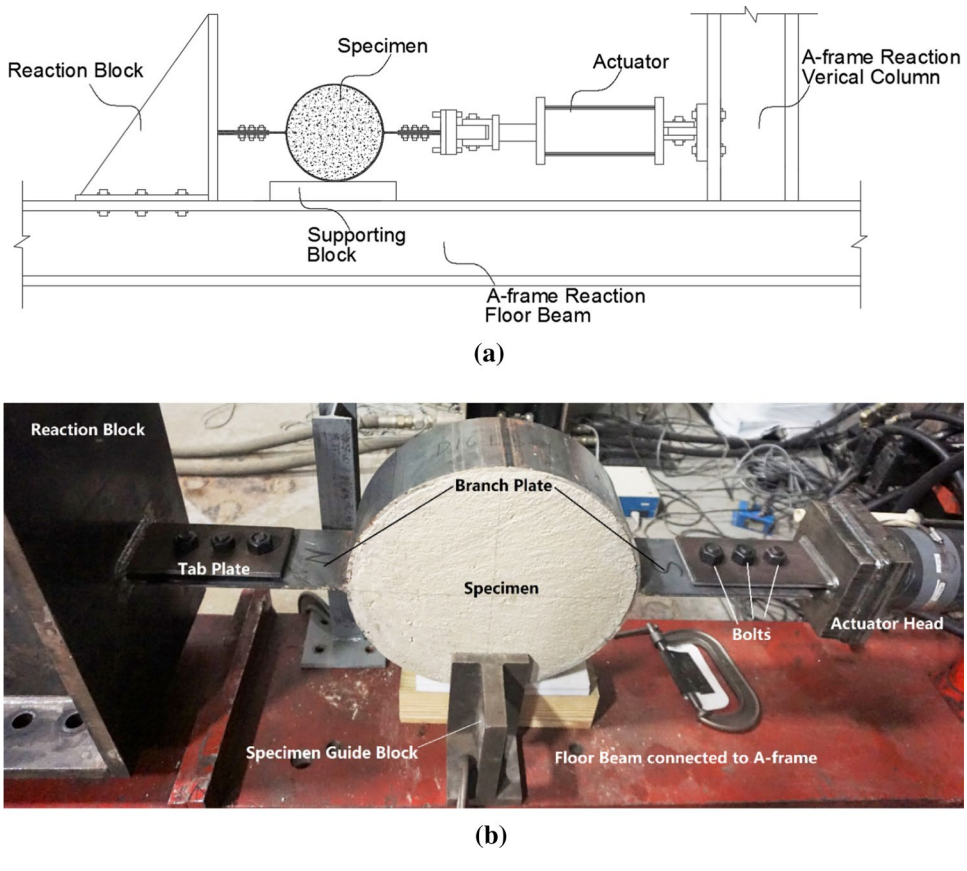

Fig. 4 Test set-up for CHS with infilled concrete specimens: **a** top view; **b** side view

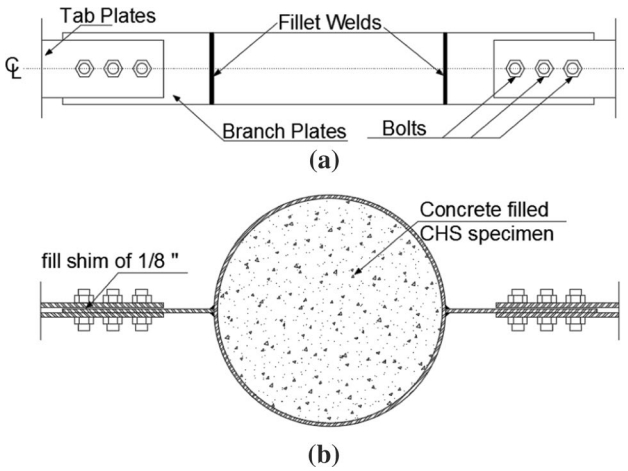

Fig. 5 CHS connections details (16″ diameter specimen): **a** top view; **b** side view

distance from the nearest bolt to the CHS fillet welds was chosen to be the equal to the length of the fillet weld, to minimize the risk of non-uniform stresses applied to the CHS by the branch plate in proximity of the bolted connections.

Final specimen dimensions are summarized in Table 1. The "D-i-L-j" nomenclature used to name the specimens refer to the diameter "i" and width "j" of the CHS used in the specimen. More than one of each specimen type was built, so that both monotonic and cyclic tests could be performed on each type of specimens. The design wall thicknesses of the CHS shapes in Table 1 are the nominal dimensions. The objective of the cyclic tests was to assess the connection behavior from a seismic application perspective if inelastic response was to develop in the CHS (i.e., for a possible connection detail used to connect BRBs to CFT bridge columns). Note that the specimen only represents the portion of the column near the connection; in other words, the portion of the column beyond the connection is not considered here. For the specimens having a 9.625″ diameter CHS (shown in Fig. 6), CHS having three different widths were tested to investigate how the strength increases as a function of the CHS and branch plate's relative width, when the CHS is not entirely welded to the branch plate. Specimens D9.625L6 and D9.625L7 were the only specimen with a CHS width larger than the branch plate width at the weld. Note that the branch plates in the specimens having CHS diameter of 14″, 9.625″, and 5″ were tapered. An example is shown in Figs. 6 for a CHS of 9.625″ diameter. The larger plate width was introduced to compensate for the cross-sectional loss at the bolt holes.

The observed performance of the first few specimens tested (as described later) dictated some minor changes to the test set-up and specimen details. Mainly: (1) the 70-kip

Table 1 Summary of specimen dimensions

Specimen name	D16L5	D14L3	D10.75L5	D9.625 L3	D9.625L6	D9.625L7	D5L3
CHS shape	16×0.25	14×0.375	10.75×0.188	9.625×0.25			5×0.25
Specimen total number	4	2	2	2	2	2	2
Design wall thickness (in)	0.233	0.349	0.174	0.233			0.233
CHS width (in)	5	3	5	3	6	7	3
Branch plate width (in)	5	3	5	3			3
Branch plate length (in)	10.5	8.5	10.5	8.5			8.5
Branch plate thickness (in)	0.25	0.375	0.25	0.375			0.375
Fillet Weld size (in)	0.25	0.375	0.25	0.375			0.375

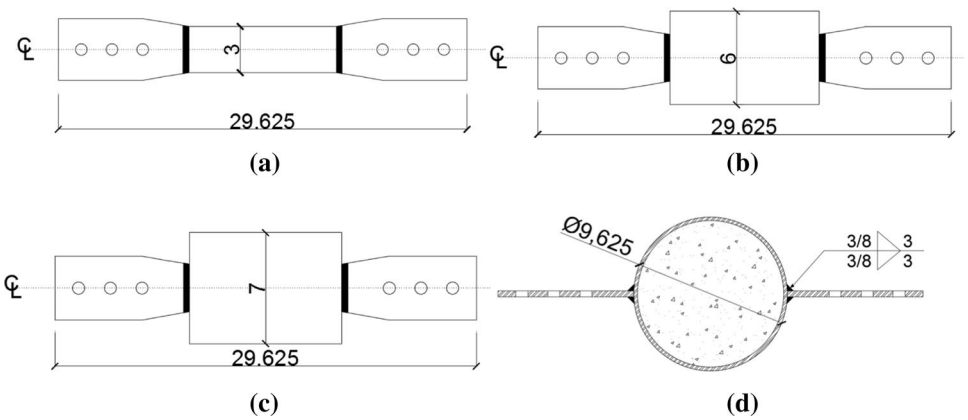

Fig. 6 Top and side views of 9.625″ diameter CHS specimens: **a** D9.625L3; **b** D9.625L6; **c** D9.625L7; **d** D9.625L3, D9.625L6 and D9.625L7 (unit: in.)

actuator initially used was replaced by one with a 250 kips capacity; (2) the branch plates for some specimens was strengthened to prevent their undesirable failure; (3) cover plates were added to one specimen to prevent non-representative concrete crushing.

Average yield strength and ultimate strength obtained from test coupons taken from each type of CHS are provided in Table 2. Concrete cylinder tests were performed to obtain the 28-day compressive strength, $f_c^{'}$. Values of 4.26, 3.82, and 4.08 ksi, were obtained from three cylinders, for an average compressive strength of 4.05 ksi (used in subsequent calculations).

Both monotonic and cyclic tests were performed using displacement control. The force was measured using internal load cells. To measure the CHS deformation in specimens, a Krypton dynamic measurement machine using Light-Emitting Diodes (LEDs recorded the 3D displacements of the specimen, the reaction block and the actuator (Fig. 7a). Additional LEDs were installed along the CHS perimeter to capture the separation of the CHS from the infilled-concrete, over a range defined by ± 45 degrees from the horizontal, as shown in Fig. 7b. The range of measurement spanned that portion of the CHS' circumference over which separation of the CHS from the concrete was anticipated (based on results from finite element analyses).

The largest deformations of the CHS (away from the concrete) was expected to happen at the CHS-to-branch plate connection points, on opposite sides of the specimen. Here, "CHS Deformation-A" refers to peak CHS deformation on the side of the actuator (obtained by the difference in the x-direction displacements measured by LEDs 5 and 12 in Fig. 7a). Similarly, "CHS Deformation-R" refers to peak CHS deformation on the side of the reaction block (obtained from the x-direction displacement difference between LEDs 4 and 12 in Fig. 7a).

Table 2 CHS steel properties (from tensile coupons)

CHS diameter	F_y (ksi)	F_u (ksi)	Maximum strain	F_u/F_y
5	64.5	71.6	0.315	1.11
9.625	47.9	65.0	0.244	1.37
10.75	48.4	61.6	0.251	1.27
14	56.0	76.1	0.329	1.36
16	50.9	70.0	0.284	1.38

5 Test Protocols

Adapted from ATC-24 (1992), the incremental cyclic test protocol pattern used here (Fig. 8) reflects that negative displacements could not be applied to the specimen because the branch plate pushes on the infilled concrete in that direction. The test protocol considered here started

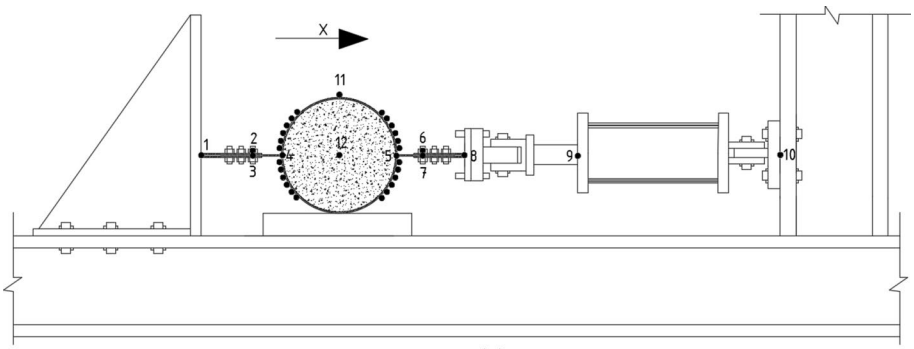

(a)

(b)

Fig. 7 Example LED layout in specimen D16L5-1 in the test set-up: **a** specimen with testing frame and LED locations; **b** close-up view of LEDs on the specimen

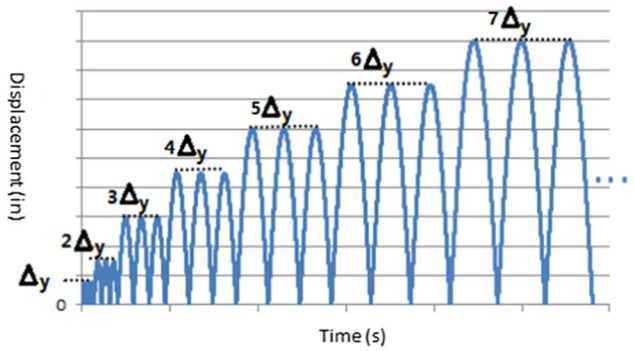

Fig. 8 Cyclic test protocol

Table 3 Test protocol yield displacement values used in incremental cyclic tests

Specimen Name	D16L5	D10.75L5	D9.625L3	D9.625L6	D9.625L7
Δ_y	0.0752″	0.0648″	0.0626″	0.0626″	0.0626″

with three cycles at the displacement level of Δ_y. Then, three cycles were applied at each of the displacement levels corresponding to $2\Delta_y$, $3\Delta_y$, $4\Delta_y$, $5\Delta_y$, $6\Delta_y$, $7\Delta_y$, etc., until specimen failure. A half-sine load vs time history was used to prevent sudden vibrations upon reversal of the direction of loading. The cyclic tests were performed at a rate of 0.4″/min (the monotonic test were four times slower). The yield displacements for the specimens (different for the various CHS of different diameters) were intended to correspond to the point when yielding first occurred anywhere on the specimen. For this purpose, the yield displacement values used to develop this protocol were those obtained from a model of the *Abaqus* specimen (because that point was hard to identify experimentally). These values used for the specimens on which cyclic tests was performed are provided in Table 3.

Table 4 summarizes the test protocols used. Hereafter, the nomenclature "D-i-L-j-k" refers to the kth specimen listed in the "Numbering" row of Table 4 for the specimen type "D-i-L-j". As part of this research program, the following tests were performed.

- Specimen D16L5-1 was tested monotonically. It failed in the branch plate. To prevent repetition of this undesirable failure mode, the branch plates of the three remaining D16L5 specimens were strengthened. Specimen D16L5-2 was then also monotonically tested. Failure this time was in the CHS close to the welds connecting the branch plate. For comparison, Specimen D16L5-3 was then subjected to repeated cycles at a constant displacement amplitude of 1.28" (this test is labelled "cyclic-2″ in Table 4). This value was arbitrarily chosen; it corresponded to the displacement of the actuator head when a force of 60 kips was applied to Specimen D16L5-2 (this being 76% of the maximum force of 79.2 kips reached in specimen D16L5-2). Finally, Specimen D16L5-4 was tested following the cyclic test protocol shown in Fig. 8.
- For D9.625L3, D9.625L6, D9.625L7, and D10.75L5, with two specimens of each type, one was tested monotonically and the other cyclically per the above protocol.
- Specimen D5L3-1 was tested monotonically. However, during that test, the infilled concrete crushed and partly fell-off at the ends of the CHS; as a result, the CHS deformed freely and fractured. The column that the specimen is intended to represent would be longer and this kind of failure would not happen due to the constraint of the column beyond the connection portion. Therefore, specimen D5L3-2 was strengthened by using cap plates on both sides of the specimen. This modification was intended to prevent the concrete from "popping out" during the CHS deformations. Then, Specimen D5L3-2 was subjected to monotonic testing; the CHS failed, again, close to the welds connecting the branch plate.
- Specimen D14L3-1 was tested monotonically. In this particular case, the concrete had been chipped at a point close to the branch plate when the specimen was installed in the test set-up. Probably as a consequence of this defect, the infilled concrete in this specimen failed before the CHS. Therefore, to get a more representative result, Specimen D14L3-2 was also tested monotonically.

Table 4 Summary of test protocols

Name	Specimen															
	D5L3		D9.625L3		D9.625L6		D9.625L7		D10.75L5		D14L3		D16L5			
CHS Diameter (in)	5		9.625		9.625		9.625		10.75		14		16			
CHS width (in)	3		3		6		7		5		3		5			
Numbering	1	2	1	2	1	2	1	2	1	2	1	2	1	2	3	4
Monotonic Test	×	×	×		×		×		×		×	×	×	×		
Incremental Cyclic Test				×		×		×		×						×
Cyclic-2 Test															×	

However, this specimen also failed in the concrete, this time because of a sudden shock induced when bolt slippage occurred.

Detailed analytical and experimental results for a few representative tests are presented below. Again, due to space constraints, not all the tested specimens are described here (details presented in Wei & Bruneau, 2016b).

6 Test of Specimens D16L5

Specimen D16L5-2 was subjected to monotonically increasing loading. The resulting force vs peak CHS displacement curve is the solid line in Fig. 9a. It is compared with the results from the *Abaqus* model of the specimen. The strength obtained from the *Abaqus* analysis was greater than the one experimentally obtained at peak CHS deformation. Figure 9a is a plot of the peak CHS deformation on the side close to the reaction block. This specimen failed at a force of 79.2 kips. Results in Fig. 9a do not extend beyond that point because failure caused sudden vibrations that caused three LEDs to fall off the CHS. In this specimen, the CHS close to the weld connecting it to the branch plate failed, on top of the branch plate on the side of the actuator. The arrow in Fig. 9b points to the CHS failure section shown in the other photo.

An incremental cyclic test was conducted on Specimen D16L5-4. From the *Abaqus* analysis, the first-yield strength for the specimen model was 10.59 kips. During the monotonic test performed on specimen D16L5-2, displacement was 0.0752″ when a force of 10.59 kips was applied. Assuming that specimens D16L5-2 and D16L5-4 were in-principle the same, specimen D15L5-4 was expected to develop the same force at first yielding. Using this yield displacement value of 0.0752″ in Table 3, the resulting cyclic loading protocol for specimen D16L5-4

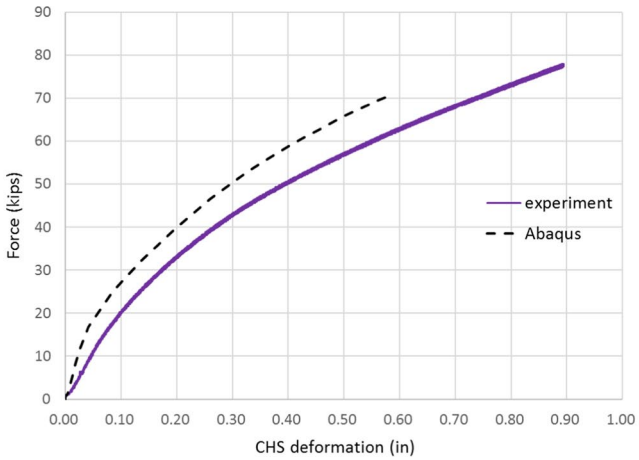

(a)

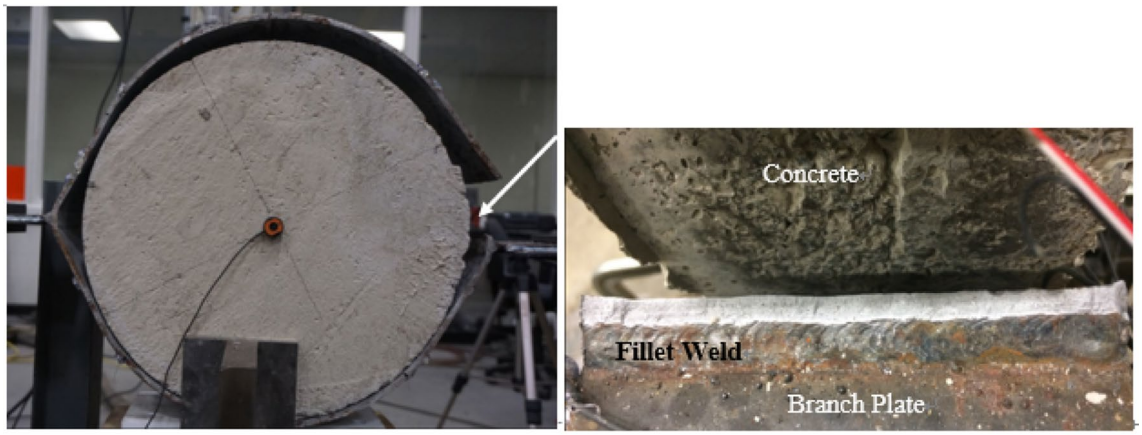

(b)

Fig. 9 Specimen D16L5-2: **a** force versus peak CHS deformation; **b** Failure of D16L5-2

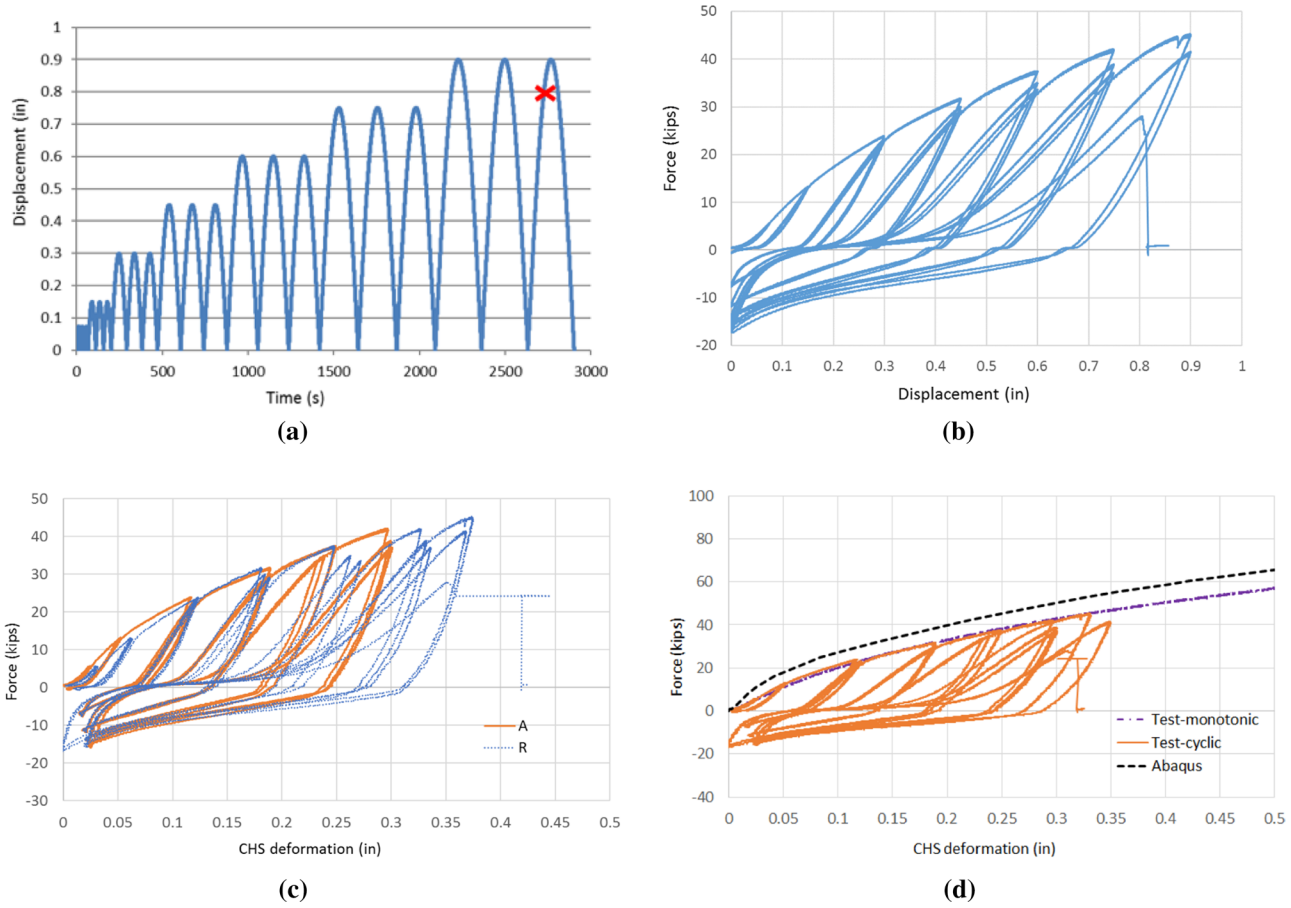

Fig. 10 Specimen D16L5-4: **a** Incremental cyclic testing protocol; **b** force vs applied displacement hysteretic curve; **c** force vs peak CHS deformation; **d** comparing test and *Abaqus* results

was developed (Fig. 10a). Failure of this specimen occurred at 7 times the yield displacement, equal to 0.81″, at the point indicated by a cross in Fig. 10a. Figure 10b shows the hysteretic force–displacement curve of the actuator head for specimen D16L5-4; the specimen developed a maximum force of 45 kips. While reloading in a subsequent cycle, at an actuator force of 27.8 kips (less than the previously reached maximum), the specimen failed in the CHS close to the weld connecting it to the branch plate. The failure section was similar to what is shown in Fig. 9b, except that, in this case, it occurred below the branch plate close to the reaction block. Figure 10c shows the force vs peak CHS deformation on both sides of specimen D16L5-4, where the labels "A" and "R" respectively refer to the peak CHS deformations on the connection sides having branch plates connected to the "Actuator" and the "Reaction block". Deformations on the actuator and reaction block sides differed slightly. Figure 10d compares the *Abaqus* analysis results with the experimentally obtained results from the monotonic testing of specimens D16L5-2 and the cyclic testing of D16L5-4. Comparison for the peak CHS deformations close to the reaction block side are used in this figure. Overall there is a good match during the first few cycles in tension between the backbone of the hysteretic curve for specimen D16L5-4 and the results for specimen D16L5-2's monotonic test. However, the analytically obtained stiffness was higher than all the experimentally obtained ones.

Note that there are some discrepancies between results for different specimens. For monotonically tested specimen D16L5-1, Fig. 11a shows the resulting force vs the peak CHS deformation. The experimentally obtained results (solid lines) are also compared with the results from the *Abaqus* model, and the results are shown to be generally close. The solid line in Fig. 11b shows the cyclic testing force vs peak CHS deformation for specimen D16L5-3 on the side close to the reaction block, which is compared with the curve from monotonic test of specimen D16L5-2 (in dash-dot line). The stiffness of specimen D16L5-3 shown in the first half cycle is less than for specimen D16L5-2. However, both two curves exhibit lower stiffness than obtained with the *Abaqus* model (dash line).

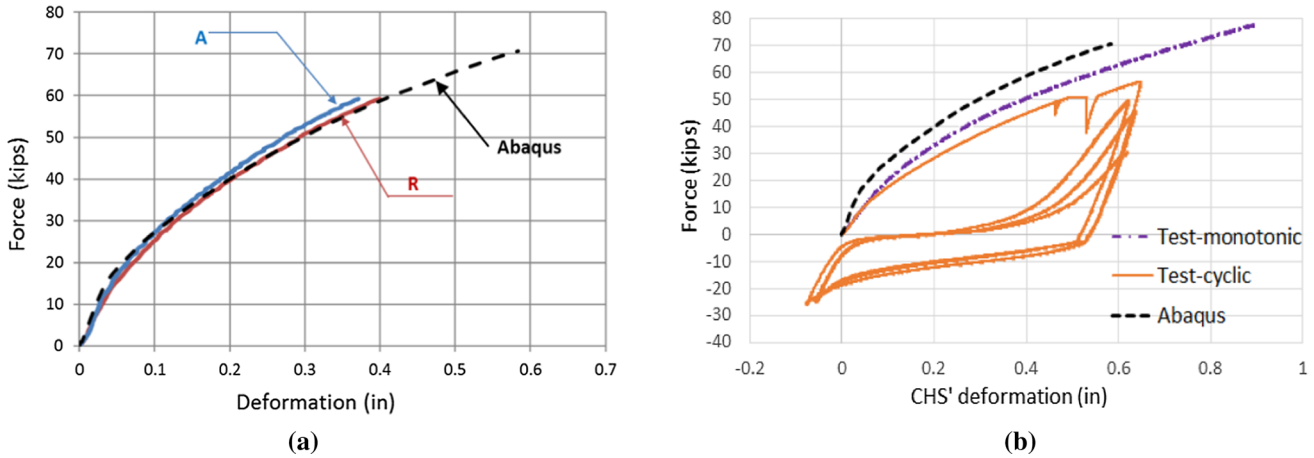

Fig. 11 Comparisons of pushover curves between *Abaqus* specimen model and test results: **a** force versus peak CHS deformation for D16L5-1; **b** force versus peak CHS deformation for D16L5-2, D16L5-3, and *Abaqus* results

7 Specimen D9.625L3, D9.625L6 and D9.625L7

The solid and dash lines in Fig. 12a show force–deformation results for Specimen D9.625L3-1, which was tested monotonically. Peak CHS deformations are provided on both sides where values were recorded. Failure occurred in the CHS close to the weld to the branch plate, when the applied force reached 44.9 kips. The *Abaqus* results for D9.625L3 are shown by the dash-dot line in this figure, and exhibits a larger stiffness than obtained experimentally.

The incremental cyclic test was performed on Specimen D9.625L3-2. The actuator's applied displacement of 0.0625″ was obtained from the monotonic test of specimen D9.625L3-1, when the first-yield strength of 5.82 kips from the *Abaqus* specimen model was applied. During the third cycle of testing at 6 times the yield displacement, the specimen failed at a displacement of 0.67″ (actuator's applied displacement). The specimen resisted a maximum force of 32.5 kips, and a force of 28.9 kips at failure of the CHS close to the weld connecting it to the branch plate (i.e., at the same location as for specimen D9.625L3-1). As shown in the force–displacement curves of Fig. 12b, for peak CHS deformations on both sides of specimen D9.625L3-2 (labeled "Cyclic-R" and "Cyclic-A"), results obtained from the monotonic test of specimen D9.625L3-1 ("Monotonic-A") match well the stiffnesses in tension.

Similarly, specimens D9.625L6 and D9.625L7 were also respectively subjected to monotonic and incremental cyclic testing. Given that the CHS width was larger than the branch

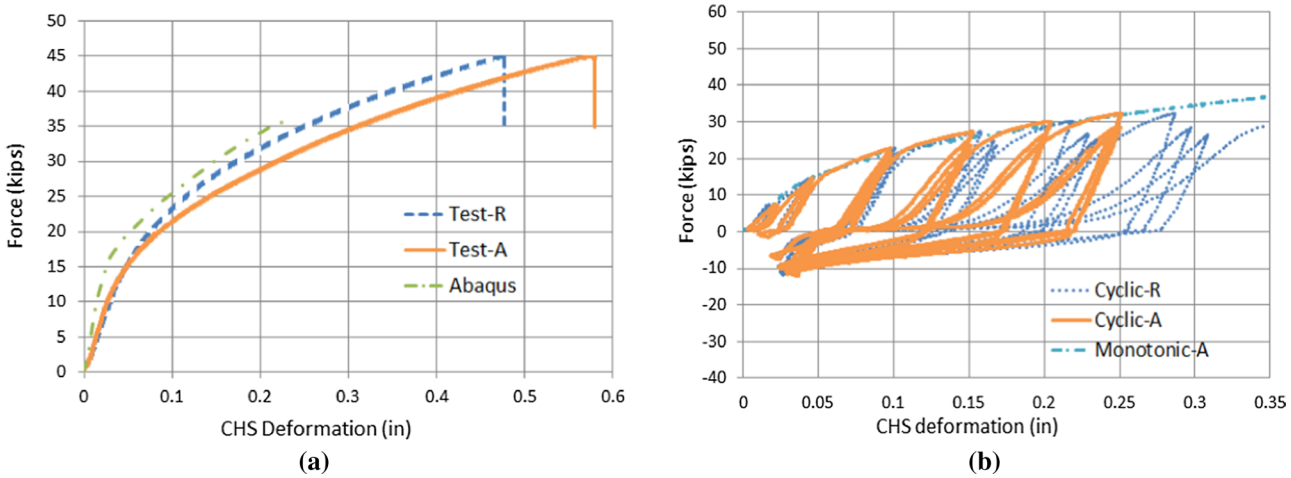

Fig. 12 Force–deformation curves for Specimen D9.625L3: **a** peak CHS deformation for D9.625L3-1; **b** peak CHS deformation of D9.625L3-1 and D9.625L3-2

plate in specimens D9.625L6 and D9.625L7, the peak CHS deformations were measured by LEDs at two different locations, as shown in Fig. 13a. The location close to the branch plate is termed "Center" in Fig. 13a, whereas the one termed "Side" was on the outside perimeter of the CHS in-line with the branch plate. The difference in deformations close and away from the branch plate can be assessed by comparing the displacements recorded at the "Center" and "Side" points. All four specimens failed in the CHS section close to the bottom of the branch plate connected to the reaction block. A typical failure section (from specimen D9.625L6-1) is shown in Fig. 13b (with specimen taken out of the test setup to provide a better picture of the failure section).

The experimentally obtained monotonic force vs CHS deformation curves obtained for specimen D9.625L6-1 are compared in Figs. 14a, b with analytical results from the corresponding *Abaqus* model D9.625L6. The labels "Test-S-A" and "Test-C-A" in Figs. 14a, b respectively refer to deformations taken at the "S" and "C" locations on the CHS close to the "Actuator" or "Reaction block" (more specifically, "S" and "C" refer to the "Side" and "Center" locations mentioned earlier). As seen in these figures, the CHS deformations were smaller when further away from the branch plate. Note that the curve for "Test-C-A" stops when the LED recording this deformation fell off the specimen (i.e., before the end of the test).

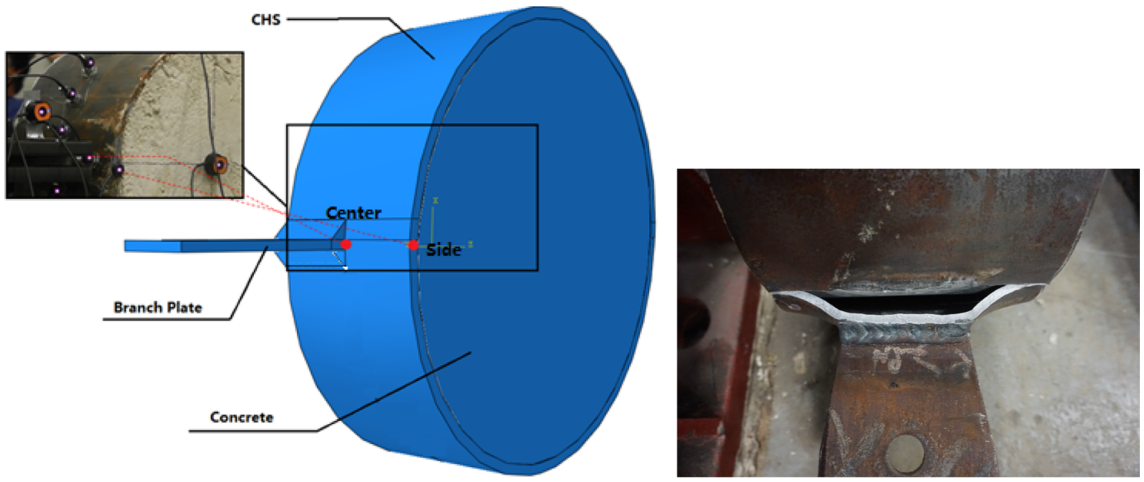

Fig. 13 Specimens D9.625L6 and D9.625L7: **a** LEDs locations to measure deformations of the CHS; **b** failure of the CHS in specimen D9.625L6-1

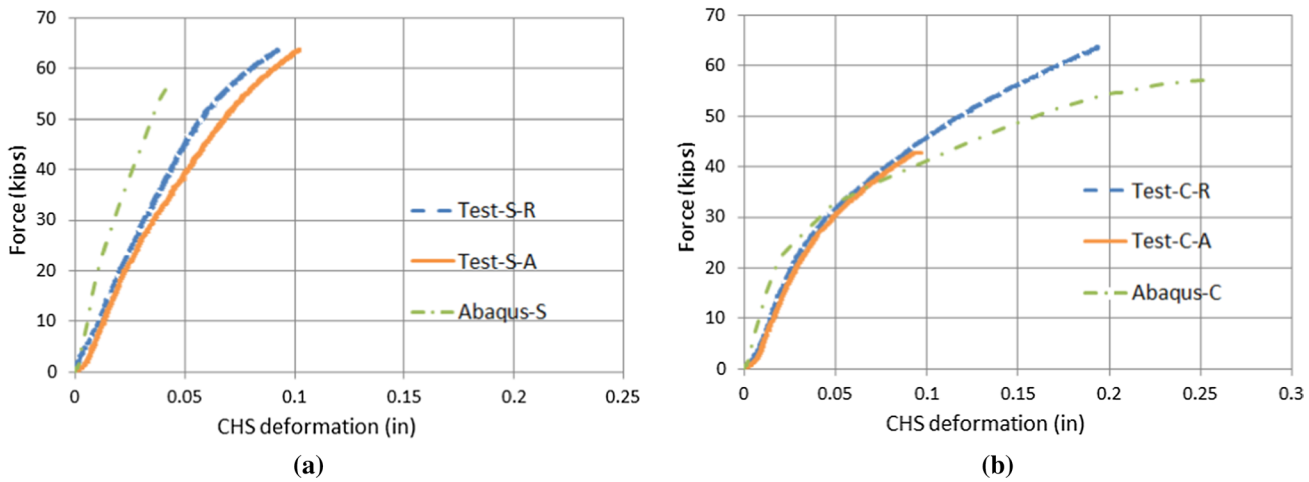

Fig. 14 Force–deformation curves for specimen D9.625L6-1: **a** at CHS "Side"; **b** at CHS "Center"

For cyclic testing of specimen D9.625L6-2, the protocol used for D9.625L3-2 was re-used to facilitate comparisons between the two specimens. During the third cycle at 6 times the yield displacement, the actuator force dropped suddenly from 37.9 to 17.4 kips, as shown in Fig. 15a, when cracking initiated in the CHS close to the weld connecting to the branch plate. Failure occurred at an actuator head displacement of 0.65″, during the first cycle at 7 times the yield displacement. The experimentally obtained applied force vs CHS deformation curves for specimens D9.625L6-1 and D9.625L6-2 are compared in Fig. 15b. These deformations are both at the "Center" location, close to the branch plate connecting to the actuator. Note that due to a data acquisition error for the LED at the "Center" location, the CHS deformation close to the branch plate connected to the reaction block was not obtained in this case. The LEDs captured CHS deformations up until to the sudden drop in force for specimen D9.625L6-2 shown in Fig. 15a. During the first few cycles in tension, there is a good match between the backbone of the hysteretic curve for specimen D9.625L6-2 and results for the monotonically tested specimen D9.625L6-1.

Monotonic and incremental cyclic tests were similarly conducted on specimens D9.625L7-1 and D9.625L7-2. Figure 16a compares the experimentally applied force versus CHS deformation obtained from the monotonic test of specimen D9.625L7-1, with the corresponding *Abaqus* analytical results for specimen D9.625L7, for deformation measured at the CHS "Center". For the incremental cyclic test performed on specimen D9.625L7-2, the applied force abruptly dropped from 46.5 kips to 17 kips during the second cycle at 6 times the yield displacement. The experimentally obtained applied force versus CHS deformations are plotted and compared in Fig. 16b for specimens D9.625L7-1 and D9.625L7-2. These CHS deformations are taken at the "Center" location, meaning close to the branch plate on both sides of the specimen. Results for specimen D9.625L7-1

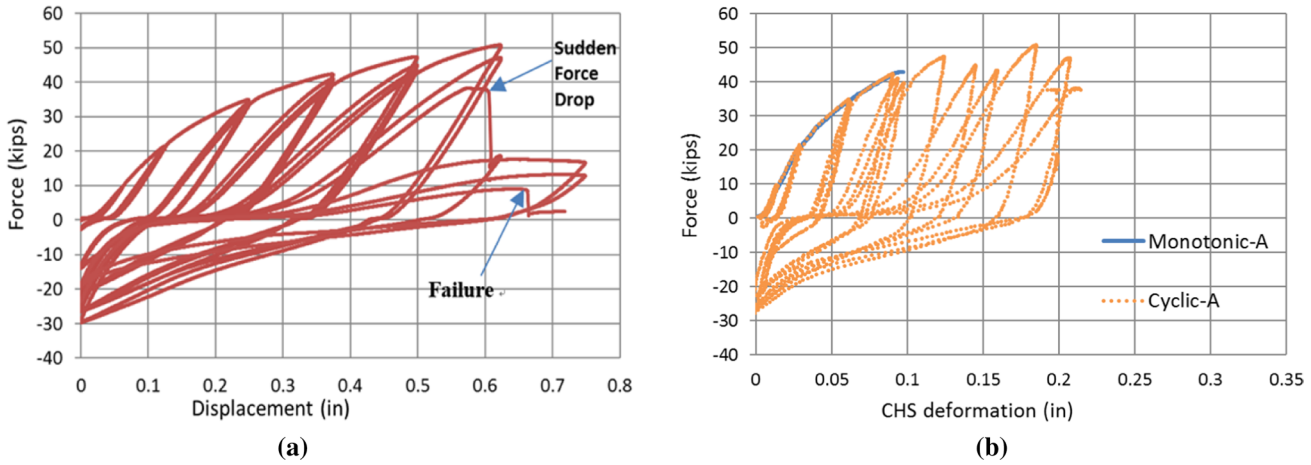

Fig. 15 Force–deformation curves for Specimen D9.625L6-2: **a** actuator's applied displacement; **b** CHS deformation curves for specimens D9.625L6-1

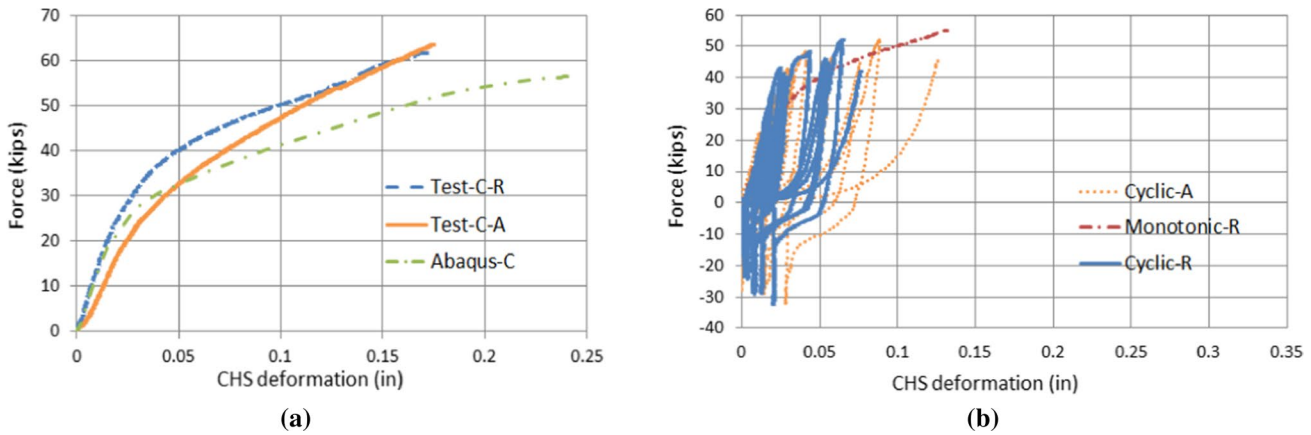

Fig. 16 Force–deformation curves at CHS "Center" of Specimen D9.625L7 compared with: **a** *Abaqus* results; **b** D9.625L7-2

Table 5 Punching shear and failure strengths for specific specimens

	Specimens						
	D5L3-1	D9.625L3-1	D10.75L5-1	D14L3-2	D16L5-2	D9.625L6-1	D9.625L7-1
Failure strength (kips)	65	44.9	54	73	79.2	63	64
f_{y0} (ksi)	64.5	47.9	48.4	56	50.9	47.9	47.9
l_1 (in)	3	3	5	3	5	3	3
t_0 (in)	0.233	0.233	0.174	0.349	0.233	0.233	0.233
Punching Shear strength (Eq. 1) (kips)	32.46	24.11	30.32	42.22	42.69	24.11	24.11
Punching Shear strength (Eq. 2) (kips)	52.30	38.84	48.85	68.01	68.79	38.84	38.84

(monotonically tested) match well with the backbone of the hysteretic curve obtained during the first few cycles in tension for specimen D9.625L7-2.

A comparison of the performance of Specimens D9.625L3, D9.625L6, and D9.626L7 shows that wider CHS provides larger strength but that their deformation capacity is significantly reduced. Note that the latter two specimens are more representative of actual branch plate-to-column connection (of the type shown in Fig. 1) because the gusset plate connecting to the CFT column is shorter than the column segment to which it connects in those cases.

8 Key Test Results and Design Implications

When comparing the plots of applied force versus CHS deformation for the specimens tested monotonically and the corresponding *Abaqus* results, a generally good match was obtained. Failure in these the specimens typically occurred close to the fillet weld of the CHS to the branch plate. For specimens D14L3 and D5L3-1, failure occurred in the infill concrete. This infill concrete crushing or popping-out of the CHS ring is not something that could occur in an actual column where the concrete is naturally, laterally restrained.

Recall that the punching shear strength can be calculated for hollow CHS-to-branch plate connections based on Eqs. 1 and 2, and Voth (2010) recommended Eq. 2, because Eq. 1 was deemed too conservative. In Table 5, the punching shear strength obtained from these two equations is compared with the strength of the specimens at failure. The monotonically tested specimens are divided into two groups: one for which the CHS and branch plate were of the same width, and the other where it was not the case. It is found that when CHS and branch plate are of identical width, the failure strength exceeded the strength obtained by Eqs. 1 and 2 by 100% and 24%, respectively.

Note that, in Table 5, the design punching shear strength for specimens D9.625L6-1 and D9.625L7-1 obtained by Eqs. 1 and 2 was calculated using the width of the branch plate rather than the full width of the CHS. The strength obtained for these two specimens in the monotonic tests were up to 165% and 65% greater than predicted by Eqs. 1 and 2. The strength of the 9.625″ diameter CHS specimen did not further increase when the width of the CHS not connected to the branch plate exceeded 6 inches. It is therefore conservative to only consider a CHS width equal to the branch plate width when calculating the strength of the specimen.

The specimens' strength under cyclic tests, beyond the first cycle, was consistently smaller than what was obtained from the monotonic tests. The hysteretic behavior also exhibited a deficient cyclic energy dissipation. On the basis of these observations, using this type of connections is not recommended for seismic applications that would push it into the inelastic range.

9 Conclusions

A gusset plates welded to CFT column connection detail was investigated. Unidirectional test results obtained could be well represented by finite element analyses of the various specimens considered. The equations proposed by Wardenier (2008) and Voth (2010) were found to give conservative results for punching shear strength when compared with the test results. However, this connection detail is not recommended if hysteretic behavior is desired under cyclic loading (such as during severe earthquakes). Future research is also needed to establish its combined shear and axial resistance before using it in the application considered here. Although the limited strength available may severely limit the applicability of this detail for the envisioned purpose, there may be other applications for which this limited strength may be adequate.

Acknowledgements The authors would like to acknowledge material donations from the Atlas Tube, JMC Steel Group of Chicago, Illinois. However, any opinions, findings, conclusions, and recommendations presented in this report are those of the writers and do not necessarily reflect the views of the sponsor.

References

Abaqus Version 6.14 [Computer software]. Dassault Systèmes Simulia Corp, RI.

American Petroleum Institute. (2007). Recommended practice for planning, designing and constructing fixed offshore platform: working stress design, 21st edition. API RP 2A, Supp 3. American Petroleum Institute (API), Dallas, USA.

ATC. (1992). Guidelines for cyclic seismic testing of components of steel structures. Report ATC-24, Applied Technology Council, Redwood City, CA.

Bauer, C. J. (1988). New standards for innovative composite construction. *Constr. Specifier, 04*, 84–89.

Fouché, P., Bruneau, M., & Chiarito, V. (2017). Dual-hazard blast and seismic behavior of concrete-filled double skin steel tubes bridge pier. *ASCE Journal of Structural Engineering*. https://doi.org/10.1061/(ASCE)ST.1943-541X.0001883

Hajjar, J. F. (2000). Concrete-filled steel tube columns under earthquake loads. *Progress in Structural Engineering and Materials, 2*(1), 72–81. https://doi.org/10.1002/(SICI)1528-2716(200001/03)2:1%3c72::AID-PSE9%3e3.0.CO;2-E

Hajjar, J. F., Gourley, B. C., Tort, C., Denavit, M. D., & Schiller, P.H. (2013), Steel-concrete composite structural systems, Department of Civil and Environmental Engineering, Northeastern University, Boston, Mass. (http://www.northeastern.edu/compositesystems)

Han, L., Li, W., & Bjorhovde, R. (2014). Developments and advanced applications of concrete-filled steel tubular (CFST) structures: Members. *Journal of Constructional Steel Research, 100*, 211–228. https://doi.org/10.1016/j.jcsr.2014.04.016

Huang, Y. (2015). Seismic behavior of concrete filled steel tubular built-up columns. Ph.D thesis, University of Trento.

Imani, R., Mosqueda, G., & Bruneau, M. (2015). experimental study on post-earthquake fire resistance of ductile concrete filled double-skin tube columns. *ASCE Journal of Structural Engineering*. https://doi.org/10.1061/(ASCE)ST.1943-541X.0001168

Kenarangi, H., & Bruneau, M. (2019a). Shear strength of composite circular reinforced concrete filled steel tubes. *ASCE Journal of Structural Engineering*. https://doi.org/10.1061/(ASCE)ST.1943-541X.0002456

Kenarangi, H., & Bruneau, M. (2019b). Experimental study on composite action in reinforced concrete filled steel tube shaft foundations. *ASCE Journal of Bridge Engineering*. https://doi.org/10.1061/(ASCE)BE.1943-5592.0001407

Kenarangi, H., & Bruneau, M. (2020). Shear strength of composite circular reinforced concrete-filled steel tubes. *Journal of Structural Engineering*. https://doi.org/10.1061/(ASCE)ST.1943-541X.0002456

Kerensky, O., & Dallard, N. (1968). The four-level interchange between M4 and M5 motorways at Almodsbury. *Proceedings of the Institution of Civil Engineers: Structures and Buildings, 40*, 295–322.

Lai, Z., Huang, Z., & Varma, A. H. (2017). Seismic analysis and performance of high strength composite special moment frames (C-SMFs). *Structures, 9*, 165–178. https://doi.org/10.1016/j.istruc.2016.12.004

Leon, R. T., Kim, D. K., & Hajjar, J. F. (2007). Limit state response of composite columns and beam-columns Part I: formulation of design provisions for the 2005 AISC specification. *Engineering Journal, AISC, 44*(1), 341–358.

Marson, J., & Bruneau, M. (2004). Cyclic testing of concrete-filled circular steel bridge piers having encased fixed-base detail. *ASCE Journal of Bridge Engineering, 9*(1), 14–23. https://doi.org/10.1061/(ASCE)1084-0702(2004)9:1(14)

Montejo, L. A., Gonzalez, L. R., & Kowalsky, M. J. (2012). Seismic performance evaluation of reinforced concrete filled steel tube pile/column bridge bents. *Journal of Earthquake Engineering, 16*(3), 401–424. https://doi.org/10.1080/13632469.2011.614678

Moon, J., Lehman, D. E., Roeder, C. W., & Lee, H. E. (2013). Strength of circular concrete-filled tubes with and without internal reinforcement under combined loading. *Journal of Structural Engineering, 139*(12), 04013012. https://doi.org/10.1061/(ASCE)ST.1943-541X.0000788

Mori, K., Hatayama, Y., Juraku, K., Katagiri, A., & Ebina, T. (2015). Designs of bridges in the Hirose-gawa area determined by competition. *IABSE Symposium Report, 104*, 1–5. https://doi.org/10.2749/222137815815774070

Packer, J. A. (1995). Concrete-filled HSS connections. *ASCE Journal of Structural Engineering, 121*(3), 458–467. https://doi.org/10.1061/(ASCE)0733-9445(1995)121:3(458)

Rabbat, B., & Russell, H. (1985). Friction coefficient of steel on concrete or grout. *Journal of Structural Engineering*. https://doi.org/10.1061/(ASCE)0733-9445(1985)111:3(505)

Roeder, C. W., Lehman, D. E., & Thody, R. (2009). Composite action in CFT components and connections. *Engineering Journal, 46*(4), 229–242.

Roeder, C., Lehman, D., & Bishop, E. (2010). Strength and stiffness of circular concrete-filled tubes. *Journal of Structural Engineering, 136*(12), 1545–1553. https://doi.org/10.1061/(ASCE)ST.1943-541X.0000263

Saini, D., & Shafei, B. (2019). Performance of concrete-filled steel tube bridge columns subjected to vehicle collision. *ASCE Journal of Bridge Engineering*. https://doi.org/10.1061/(ASCE)BE.1943-5592.0001439

SAP2000 Version 14 (Computer software). Computers & Structures. Inc, CA.

Tarics, A. G. (1972). Concrete-filled steel columns for multistory construction. *Modern Steel Constr., 12*, 12–15.

Vargas, R., Bruneau, M. (2006). Analytical investigation of the structural fuse concept, Technical Report MCEER-06-0004, Multidisciplinary Center for Earthquake Engineering Research, State University of New York at Buffalo, Buffalo, NY.

Viest, I. M., Colaco, J. P., Furlong, R. W., Griffis, L. G., Leon, R. T., & Wyllie, L. A., Jr. (1997). *Composite construction design for buildings*. American Society of Civil Engineers and McGraw-Hill.

Vogeli, R. (1950). New transmission lines with concrete filled steel tube towers. Proceedings - International Conference on Large Electric Systems, (Vol. 2, p. 223).

Voth, A. P. (2010). Branch plate-to-circular hollow structural section connections. Ph.D. thesis, University of Toronto, Toronto, Canada.

Wardenier, J., Kurobane, Y., Packer, J. A., van der Vegte, G.J., & Zhao, X.-L. (2008), Design guide for circular hollow section (CHS) joints under predominantly static loading, 2nd Edition, CIDECT, Geneva, Switzerland.

Wardenier, J., Packer, J. A., Zhao, X.-L. & van der Vegte, G.J. (2010). Hollow sections in structural applications. (2nd Ed.), CIDECT and Bouwen met Staal, Rotterdam, The Netherlands.

Webb, J., & Peyton, J. J. (1990). Composite concrete filled steel tube columns. Second National Structural Engineering Conference 1990: Preprints of Papers, *1*(1), 181–185.

Wei, X., & Bruneau, M. (2016a). Case study on applications of structural fuses in bridge bents. *ASCE Journal of Bridge Engineering*. https://doi.org/10.1061/(ASCE)BE.1943-5592.0000854

Wei, X., & Bruneau, M. (2016b). Buckling restrained braces applications for superstructure and substructure protection in bridges, Technical Report MCEER-16-0009, MCEER, University at Buffalo, Buffalo, NY.

Xiao, C., Cai, S., Chen, T., & Xu, C. (2012). Experimental study on shear capacity of circular concrete filled steel tubes. *Steel and Composite Structures, 13*(5), 437–449. https://doi.org/10.12989/scs.2012.13.5.437